Available online at www.sciencedirect.com
SCIENCE DIRECT®
Advances in Space Research 35 (2005) 2141–2146
ADVANCES IN SPACE RESEARCH (a COSPAR publication)
www.elsevier.com/locate/asr

Solar wind electron density and temperature over solar cycle 23: Thermal noise measurements on Wind

K. Issautier [a,*], C. Perche [a], S. Hoang [a], C. Lacombe [a], M. Maksimovic [a], J.-L. Bougeret [a], C. Salem [b]

[a] Observatoire de Paris, LESIA, 5 place Jules Janssen, UMR 8109 CNRS, 92195 Meudon, France
[b] Space Sciences Laboratory, University of California, Berkeley, CA 94720, USA

Received 29 October 2004; received in revised form 6 April 2005; accepted 25 April 2005

Abstract

We present the solar wind plasma parameters obtained from the Wind spacecraft during more than nine years, encompassing almost the whole solar cycle 23. Since its launch in November 1994 Wind has frequently observed the in-ecliptic solar wind upstream of the Earth's bow shock. The WIND/WAVES thermal noise receiver was specially designed to measure the in situ plasma thermal noise spectra, from which the electron density and temperature can be accurately determined. We present and discuss histograms of such measurements performed from 1994 to 2003. Using these large data sets, we study the density and core temperature variations with solar activity cycle and with different regimes of the solar wind. We confirm the anticorrelation of the electron density with the sunspot number, and obtain a positive correlation of the core temperature, with the sunspot number.

Keywords: Solar wind; In situ diagnostics; Electron density and temperature measurements; Solar activity; Plasma; Wind spacecraft

1. Introduction

Knowledge of the solar wind electron density N_e and core temperature T_c is essential to study the solar and heliospheric activity and its variations with time and space. A good opportunity to get such parameters continuously and at high time resolution has been offered by the Wind spacecraft, which has observed the solar wind plasma for ten years, in the ecliptic plane upstream of the Earth's bowshock, near 1 AU. From the thermal noise receiver (TNR) of the WAVES experiment on Wind, several plasma parameters can be determined using the quasi-thermal noise (QTN) spectroscopy (Meyer-Vernet and Perche, 1989). This method mainly yields N_e with an accuracy of a few percent, and T_c.

In the following, we briefly describe the TNR on Wind and the data reduction based on the QTN spectroscopy. The present work is an extension of the paper of Salem et al. (2003) based on a restricted data set. Here, we present the histograms using a ten-year data set of N_e and T_c, acquired on Wind between 1994 and 2003, and also perform the solar wind speed histogram measured by particle analyzer. In addition, we focus on their variations with the sunspot number over the solar cycle 23.

2. Observations and data reduction

We use radio spectra acquired by the TNR, which is a part of the WAVES experiment (Bougeret, 1995) on Wind. This receiver is connected to the 2×50-m thin wire electric dipole antenna in the spacecraft spin plane. The TNR was mainly designed to measure the thermal

* Corresponding author. Tel.: +33 1 45 07 76 67; fax: +33 1 45 07 28 06.
E-mail address: karine.issautier@obspm.fr (K. Issautier).

0273-1177/$30
doi:10.1016/j.asr.2005.04.085

electric noise in the solar wind around the electron plasma frequency f_p, where f_p (kHz) $\simeq 9\sqrt{N_e\ (\mathrm{cm}^{-3})}$. Most of the time, TNR measures the thermal noise spectrum on 96 frequency channels logarithmically spaced between 4 and 256 kHz and acquired simultaneously in 4.5 s.

The QTN method consists in measuring the electrostatic fluctuations produced on the antenna by the thermal motion of the ambient electrons and protons. Since the theoretical spectrum depends directly on the particle velocity distribution functions (VDF), for the electrons we assume a sum of two isotropic Maxwellian distributions, a core (density N_c, temperature T_c) and a halo (density N_h, temperature T_h). This model for the electron VDF has shown to be a good approximation for the observed electron distribution in the solar wind (Feldman et al., 1975). For the protons, we assume a single drifting Maxwellian (solar wind speed V_{sw}, temperature T_p). The fit of the QTN model to each measured spectrum gives the six mentioned parameters: $N_e = N_c + N_h$, T_c, N_h/N_c, T_h/T_c, V_{sw} and T_p. In particular, it yields an accurate determination of N_e, since it relies essentially on the location of f_p in the spectrum, which is nearly independent of the receiver gain calibration. In addition, this method can provide accurate T_c measurements (Issautier et al., 2001). Specific applications of this method on Wind were described by Maksimovic et al. (1998) and by Salem et al. (2001, 2003). A typical example of the voltage power spectrum observed by Wind along with the fitted model spectrum is shown in Fig. 1 of Salem et al. (2003).

In the specific case of Wind with its high time resolution data acquisition, to improve the speed of the QTN fit procedure we fix the V_{sw} and T_p parameters with their values measured by the proton electrostatic analysers from the 3-D Plasma (3-DP) experiment (Lin et al., 1995). Moreover, the identification of the plasma line f_p is done by the neural network, specially developed for TNR (Richaume, 1996). It is important to note that the neural network only uses the location of the cut-off of the plasma line in the noise spectrum, independently of any electron distribution model. It is used as a guessed value of f_p to enhance the speed of the fitting procedure. Combined with the V_{sw} and T_p from 3-DP, this improves the overall fitting process and the accuracy on the resulting parameters. It is noteworthy the neural network density n_{nn} is in good agreement with the value obtained by the fit n_{QTN}. As an illustration, a 2-D histogram scatterplot of n_{QTN} and n_{nn} is plotted in Fig. 1. Their excellent accordance is shown by the corresponding correlation coefficient, which is close to 1. The associated regression line (dotted line in Fig. 1) is given by $n_{nn} = 0.97 n_{QTN} + 0.86$. Also, the histogram of the difference $\Delta N_e/N_e = 100(n_{e(nn)} - n_{e(QTN)})/n_{e(QTN)}$, which quantifies the agreement of the two data sets, has a mean around -0.46% and a standard deviation of

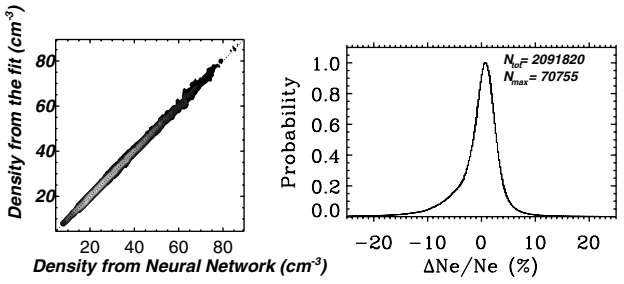

Fig. 1. (Left) 2-D histogram scatterplot of N_e deduced from the neural network n_{nn} and the fitting procedure n_{QTN}, during almost ten years of the mission. One can see that the agreement is very good since the correlation coefficient is 0.99. (Right) Histogram of the difference ΔN_e (see text). N_{tot} indicates the total number of data used to make the histogram while N_{max} indicates the number of points at the peak of the distribution.

4.31%. Note that 95% of the data are between -9.5% and $+6.3\%$.

For the present study, we use the TNR data acquired near 1 AU between 11 November 1994 and 31 December 2003, including the 1996 solar minimum and the 2001 solar maximum of the solar cycle 23. In the data reduction process, we only consider 4.5-s spectra taken every minute, and time intervals when Wind (at the GSE position X, Y, Z) was reliably upstream of the Earth's bow shock, i.e., $X > X_{shock}$. For X_{shock}, we assumed a model $X_{shock} = 30(1 - (Y_{GSE}^2 + Z_{GSE}^2)/50^2)$ that is much further from Earth than the usually observed shock positions (all lengths are expressed in Earth's radii). In order to minimize pollution from non-thermal emissions, a numerical algorithm is first applied to automatically eliminate any portions of spectra that are affected. Finally, upper limits are imposed on the fit rms error σ and parameter uncertainties for the data to be retained for analysis: $\sigma < 5\%$ for all data; in addition for N_e, $\sigma_{N_e} < 12\%$ and for T_c, $\sigma_{T_c} < 40\%$.

3. Histograms of plasma parameters

On Wind, we have obtained a large data set of nearly 2 millions of measurements acquired in the solar wind near 1 AU, over almost the whole solar cycle 23. This large data set is therefore well suited to statistically study the different regimes of the solar wind in the ecliptic plane. Fig. 2 shows the resulting histograms of N_e and T_c, measured by the QTN, and V_{sw} measured by the 3-DP. One can see that the histograms have a complex distribution. In Fig. 2, the shape of the N_e and T_c histograms strongly suggests to fit them with a sum of 3 Gaussian distributions; the resulting fits are shown by solid lines. Attempts to fit both N_e and T_c distributions with only 2 Gaussians significantly increase the χ^2 or rms error σ of the fit. On average, the N_e histogram has a mean of 9.4 cm^{-3}, and the T_c histogram has a

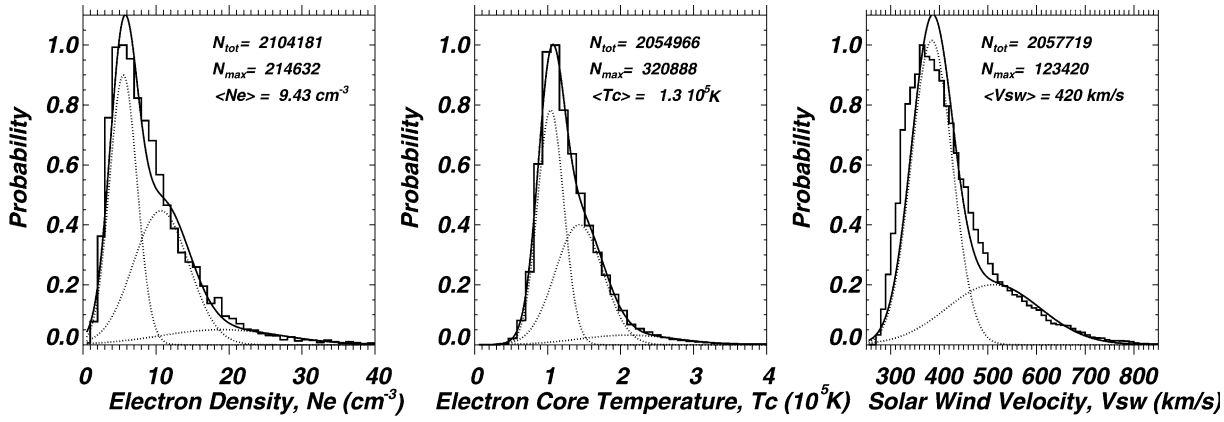

Fig. 2. Histograms of N_e, T_c and V_{sw} obtained from November 1994 to December 2003. We indicate the total number of data used to make the histogram (N_{tot}), the number of points at the peak (N_{max}), and the mean of the parameter over the whole period. The 3-Gaussian fit to the observed histograms is shown by a continuous line and individual Gaussians by dotted lines (see Table 1 for the result summary). The V_{sw} histogram is fitted with 2 Gaussians corresponding to the fast and slow wind, respectively.

mean of 1.27×10^5 K. Table 1 summarizes the results of the 3-Gaussian fits to the observed histograms. From Fig. 2, the mean values of T_c are compatible with those obtained by Salem et al. (2003), whereas the mean values of N_e are larger than those reported by these authors. The shapes of individual 1-year histograms of N_e,T_c, and V_{sw} (not shown) remain similar over solar cycle 23. However, it is worth noting that the histograms of T_c obtained in 1996, 1997, 2001 and 2003 could not be fitted with 3 Gaussians, the third population being too small to be significantly fitted.

Our multi-Gaussian fit to the observed N_e and T_c histograms points to a classification of the solar wind flow into 3 main populations in N_e and 3 main populations in T_c, as already discussed in Salem et al. (2003) for ineclitic observations. The density populations are likely to be associated with 3 major classes of solar wind: (i) the 'quiet' undisturbed wind with lower mean values of N_e (Gaussian 1); (ii) the denser heliospheric plasma sheet with intermediate values of N_e (Gaussian 2); (iii) the overdense 'disturbed wind' with interplanetary shocks, density compressions regions, etc. (Gaussian 3), with higher mean values of N_e. The histogram of V_{sw} reveals only two main types of flows in the ecliptic plane over solar cycle 23, in agreement with previous works (e.g. Neugebauer (2001)). It is fitted with two Gaussians, corresponding to the slow and fast wind, respectively. Indeed, some structures of the solar wind may have similar speed characteristics for a given density and/or temperature data set. Note that the way in which the characteristics of these populations varies over the course of a solar cycle will be further discussed in the next section.

While the 3 Gaussian components of the histogram of N_e correspond to different types of structure in the solar wind, the 3 Gaussian components of the histogram of T_c are more difficult to associate to specific structures. In particular, many interplanetary events from N_e populations 2 and 3 could be associated with T_c populations 1, 2, or 3. Salem et al. (2003) have discussed ways to examine the relationship between N_e and T_c. Fig. 3 shows distributions of T_c for 3 populations of N_e determined, corresponding to the mean value ± the standard deviation of the 3 Gaussian components listed in Table 1. These three distributions of T_c do not resemble the three Gaussian components of T_c from Fig. 2. Instead, these populations appear to have a non-Gaussian distribution and are slightly separated, with their peak values ranging around 10^5 K and slightly decreasing with denser N_e distributions (slight anticorrelation between N_e and T_c). For T_c, the mean values are around 1.18×10^5 K (for density range 1), 1.08×10^5 K (for range 2) and 1.02×10^5 K (for range 3). Doing the same analysis for V_{sw}, we find a well-known anticorrelation between N_e and V_{sw}: the lower values of V_{sw} correspond to the higher values of N_e and vice-versa. For V_{sw}, the

Table 1
Wind histograms for the solar wind electron density, core temperature, and solar wind speed measured from 1994 to 2003

Parameters of Gaussian distribution functions fitted to histograms	Gaussian 1		Gaussian 2		Gaussian 3	
	Mean	Standard deviation	Mean	Standard deviation	Mean	Standard deviation
Density N_e (cm^{-3})	5.52	1.88	10.68	3.8	18.90	8.30
Temperature T_c (10^5 K)	1.05	0.18	1.43	0.33	2.10	0.66
Speed V_{sw} (km/s)	385	42	512	96		

We indicate the mean and the standard deviation for each fitted Gaussian.

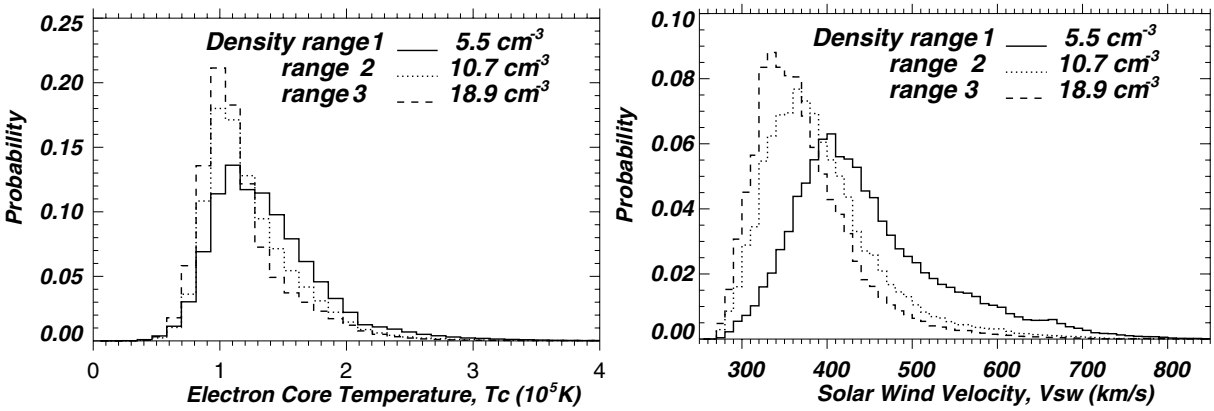

Fig. 3. Histograms of T_c and V_{sw} for the 3 fitted Gaussians in N_e obtained for nine years (labelled density range 1, range 2 and range 3, respectively), normalized by the total number of data in each histogram. For each histogram we consider the population for which N_e is within the interval [mean value ± standard deviation] as given in Table 1. For T_c, the mean values of the histograms are around 1.18×10^5 K (for density range 1), 1.08×10^5 K (for density range 2) and 1.02×10^5 K (for density 3). For V_{sw}, the mean values of the histograms are around 448 km/s (for range 1), 394 km/s (for range 2) and 373 km/s (for range 3).

mean values are around 448 km/s (for density range 1), 394 km/s (for range 2) and 373 km/s (for range 3). Note the larger spread and the higher peak value of the V_{sw} histogram associated with the lower values of N_e (solid line): at solar minimum and at high latitudes Ulysses has confirmed the solar wind structure reduces essentially to a single population in N_e and T_c, corresponding to the fast steady-state wind flowing from polar coronal holes (Issautier et al., 1998).

4. Variations of solar wind parameters with solar cycle

Fig. 4 represents the variations with time of the mean values of N_e, T_c and V_{sw} obtained every year (black solid line). In addition, we plot the mean value of each fitted Gaussian of the yearly histograms by a grey dotted line for Gaussian 1, a grey dashed line for Gaussian 2 and a grey dash-dotted line for Gaussian 3, respectively. For N_e (top panel), Gaussian 1 (grey dotted line) and Gaussian 2 (grey dashed line) vary with time. After 1998 the intermediate population, mainly the heliospheric plasma sheet (grey dashed line), merges into the mean average density (black solid line). For the fitted Gaussians of T_c (middle panel), Gaussian 1 and Gaussian 2 follow the same variation in time as the yearly averaged value (black solid line). One can see an increase of the mean values for both Gaussians after 2000. As previously discussed, since the 3-Gaussian fit could not be done every year, there is no mean values for the T_c Gaussian 3 (dash-dotted line) in 1996, 1997, 2001 and 2002. The temperature is on average cooler near solar minimum, with a 20% variation from minimum (in 1996) to maximum (in 2001). The bottom panel shows the variation of the solar wind speed. Both fitted Gaussians follow the same weak variation as the mean value (black solid line). Our results can be compared to large-scale variations of

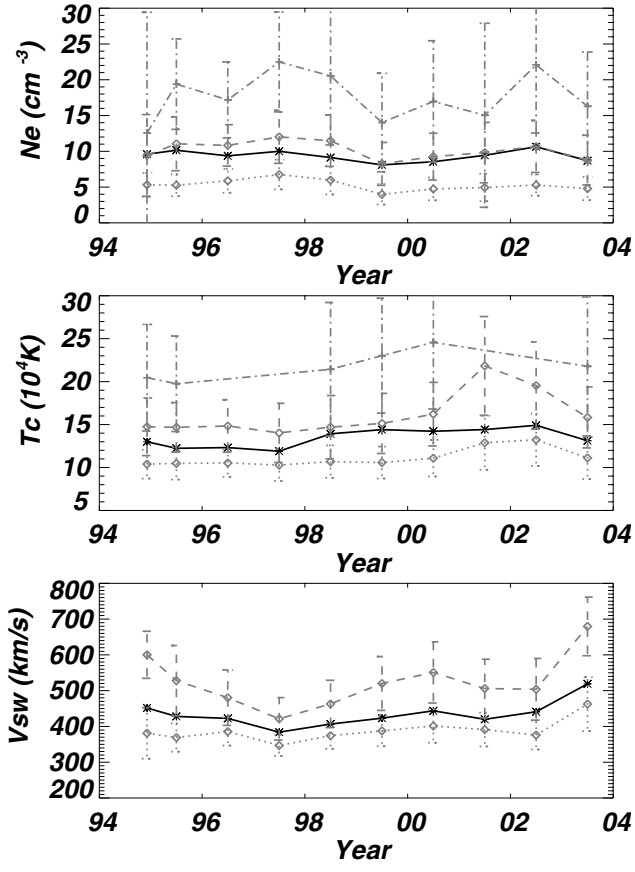

Fig. 4. Time variations of the yearly averaged N_e, T_c and V_{sw} (black solid line) during the first nine years of the Wind mission at 1 AU. The mean values of each Gaussian of Fig. 2 are also displayed. Statistical errors are given as vertical bars on each averaged data.

the mean proton density and solar wind speed, reported by Richardson and Wang (1999), combining IMP8, Voyager 2 and Ulysses measurements from 1988 to 1998.

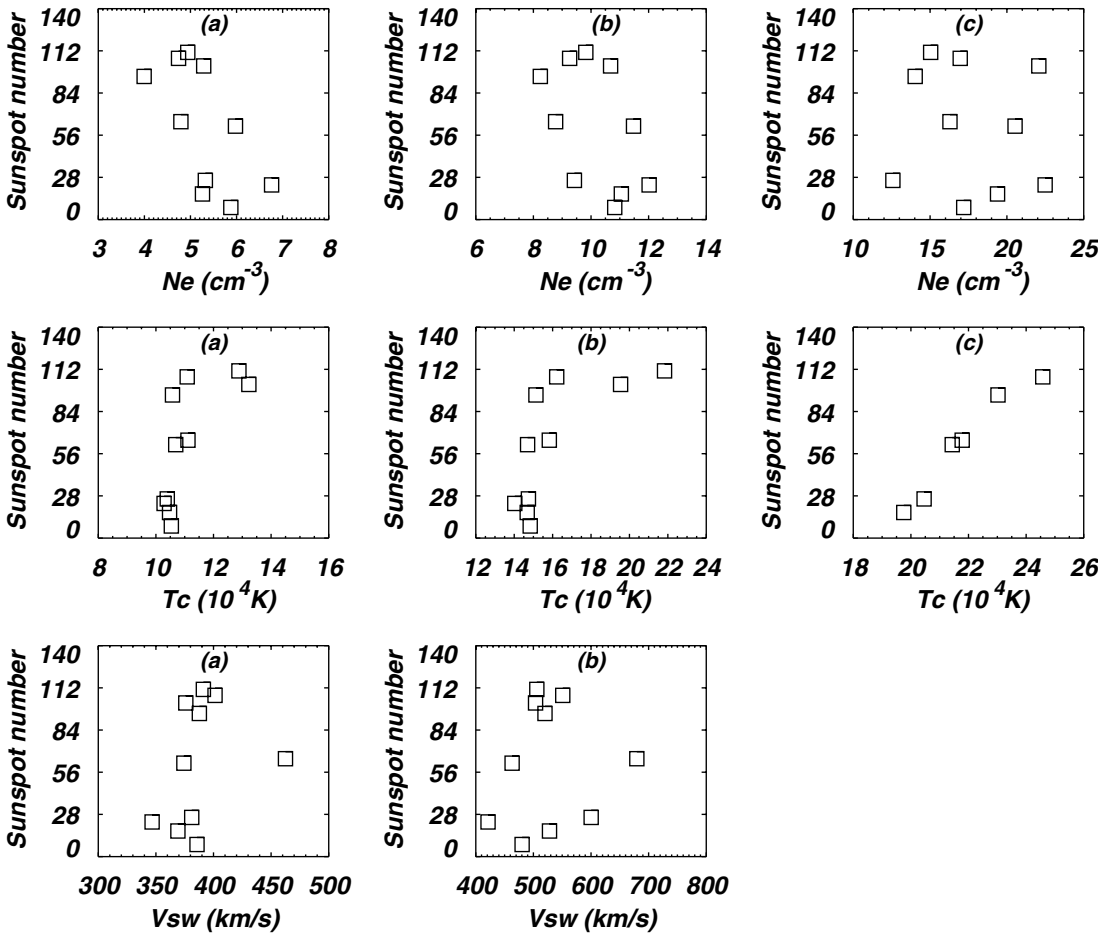

Fig. 5. Correlation of the fitted Gaussians of the solar wind N_e, T_c, and V_{sw} with sunspot number of solar cycle 23. The 1-year averaged parameters are plotted. The three columns a, b and c correspond to the three Gaussians 1, 2 and 3.

Fig. 5 shows the correlation of the N_e, T_c and V_{sw} yearly averages for each fitted Gaussian distribution with the sunspot number. Considering N_e, we note its well-known anticorrelation with solar cycle (Schwenn, 1983): the top panels reveal that the most dilute population of N_e (Gaussian 1) and the intermediate one (Gaussian 2) significantly depend on solar cycle. Indeed, Gaussian 1 is partially attributed to the fast and dilute wind coming from high-speed wind originating from coronal holes (Issautier et al., 2004). The location and shape of coronal holes are indeed very dependent on solar activity (Luhmann et al., 2002). The mean values of these N_e distributions are higher at solar minimum (low sunspot number) than at maximum (high sunspot number). In the ecliptic plane the solar wind is thus denser near solar minimum than near solar maximum. This conclusion is less clear for the third population (labelled (c) on the Figure). Note that it is important to separate the different populations for this study, the anticorrelation being less clear for the global mean value. With regard to T_c (middle panels), we find some correlation with solar cycle, more or less for the 3 fitted Gaussians. In the ecliptic plane, the solar wind appears hotter near solar maximum than near solar minimum. It is important to note that the strongest correlation is for the hotter population (Gaussian 3 in Table 1). This population contains overdense disturbed wind, including density compression regions, solar transient events, etc. These high temperature events are indeed more frequent during solar maximum due to solar activity. Considering the solar wind speed, we do not find any clear correlation with sunspot number although one might see a spread into 2 populations in the bottom panel (b).

5. Conclusion

Since its launch in 1994, the Wind thermal noise receiver has frequently recorded in-ecliptic solar wind radio spectra, from which accurate measurements of the total electron density N_e and core temperature T_c are obtained using the QTN spectroscopy. The large sample of N_e and T_c data points (~2 millions) allows us to study the solar wind structure with the solar activity. In the ecliptic

plane the solar wind reveals a complex distribution for both N_e and T_c pointing to a mixture of different regimes of wind. On average, we found that the solar wind is cooler (by 20%) and denser (by 15%) at solar minimum than at solar maximum, in agreement with studies of Salem et al. (2003) and Issautier et al. (2004). Note that large-scale variations combining IMP-8, Ulysses and Voyager 2 proton density and speed measurements are reported by Richardson and Wang (1999) from 1988 to 1998. We have confirmed an anticorrelation of the electron density with the sunspot number during solar cycle 23 for the most dilute population. Note the importance to separate the different populations of density, the anticorrelation being less clear for the global mean value. In addition, we have obtained a positive correlation for T_c with the sunspot number. The mean value of T_c is about 1.23×10^4 K near the 1996 solar minimum whereas it is around 1.44×10^4 K near the 2001 solar maximum. The strongest correlation is obtained for the hottest population of the solar wind. This latter population includes overdense disturbed wind events, which are indeed more frequent during solar maximum due to solar activity.

Acknowledgements

The Wind/WAVES investigation is a collaboration of the Observatoire de Paris, NASA/GSFC and the University of Minnesota. The 3-D Plasma Instrument is a joint effort of the Space Sciences Laboratory (Berkeley), the University of Washington, the CESR (Toulouse, France), ESTEC (the Netherlands), and the Max Planck Institute (Germany). The French contribution to the Wind project is supported by the CNES and CNRS. Special thanks to R.P. Lin for the use of the 3-D Plasma measurements.

References

Bougeret, J.-L. et al. WAVES: the radio and plasma wave investigation on the WIND spacecraft. Space Science Reviews 71, 231–263, 1995.

Feldman, W.C., Asbridge, J.R., Bame, S.J., Montgomery, M.D., Gary, S.P. Solar wind electrons. J. Geophys. Res. 80, 4181–4196, 1975.

Issautier, K., Meyer-Vernet, N., Moncuquet, M., Hoang, S. Solar wind radial and latitudinal structure: electron density and core temperature from Ulysses thermal noise spectroscopy. J. Geophys. Res. 103, 1969, 1998.

Issautier, K., Skoug, R., Gosling, J., Gary, S., McComas, D. Solar wind plasma parameters on Ulysses: detailed comparison between Swoops and Urap experiments. J. Geophys. Res. 106, 15, 2001, 665–15,675.

Issautier, K., Moncuquet, M., Hoang, S. Solar wind electron parameters from Ulysses/Urap quasi-thermal noise measurements at solar maximum. Solar Phys. 221, 351–359, 2004.

Lin, R.P., Anderson, K.A., Ashford, S., et al. A three-dimensional plasma and energetic particle investigation for the Wind spacecraft. Space Sci. Rev. 71, 125–153, 1995.

Luhmann, J.G., Li, Y., Arge, C.N., et al. Solar cycle changes in coronal holes and space weather cycles. J. Geophys. Res. 107 (SMP 3-1). doi: 10.1029/2001JA007550, 2002.

Maksimovic, M., Bougeret, J.-L., Perche, C., Steinberg, J.T., Lazarus, A.J., Vinas, A.F., Fitzenreiter, R.J. Solar wind density intercomparisons on the WIND spacecraft using WAVES and SWE experiments. Geophys. Res. Lett. 25, 1265–1268, 1998.

Meyer-Vernet, N., Perche, C. Tool kit for antennae and thermal noise near the plasma frequency. J. Geophys. Res. 94, 2405, 1989.

Neugebauer, M. The solar-wind and heliospheric magnetic field in three dimensions, in: Balogh, A., Marsden, R.G., Smith, E.J. (Eds.), The Heliosphere near Solar Minimum. The Ulysses Perspective. Springer-Praxis Books in Astrophysics and Astronomy, London, pp. 43–106, 2001.

Richardson, J., Wang, C. The global nature of solar cycle variations of the solar wind dynamic pressure. Geophys. Res. Lett. 26, 561–564, 1999.

Richaume, P. Approche connexionniste pour le pilotage temps réel du récepteur numérique Waves/TNR embarqué sur la sonde spatiale Wind, PhD Dissertation, Conservatoire National des Arts et Métiers, Paris, France, 1996.

Salem, C., Bosqued, J.-M., Larson, D.E., Mangeney, A., Maksimovic, M., Perche, C., Lin, R.P., Bougeret, J.-L. Determination of accurate solar wind electron parameters using particle detectors and radio wave receivers. J. Geophys. Res. 106, 21701–21717, 2001.

Salem, C., Hoang, S., Issautier, K., Maksimovic, M., Perche, C. Wind–Ulysses in situ thermal noise measurements of solar wind electron density and core temperature at solar maximum and minimum. Adv. Space Res. 32, 491–496, 2003.

Schwenn, R. The average solar wind in the inner heliosphere: Structures and slow variations. in: Neugebauer, M. (Ed.), Solar Wind Five, vol. CP-2280. NASA Conference Publication, pp. 489–507, 1983.